

**Proceedings of the
VIIIth International Workshop on
Heavy Quarks and Leptons
HQL06**



October 2006

Deutsches Museum, Munich

Editors

S. Recksiegel, A. Hoang, S. Paul

Organized by the Physics Department of the Technical University of Munich
and the Max-Planck Institute for Physics, Munich

**This document is part of the proceedings of
HQL06, the full proceedings are available from
<http://hql06.physik.tu-muenchen.de>**

Leptonic and Semileptonic D -Decays

Hanna Mahlke
Laboratory of Elementary-Particle Physics
Cornell University
Ithaca, NY 14853
USA

1 Introduction

The study of semileptonic and leptonic decays allows the determination of fundamental parameters of the Standard Model (SM), which are related to the elements of the Cabibbo-Kabayashi-Maskawa matrix. Examples of these processes are shown in Fig. 1.

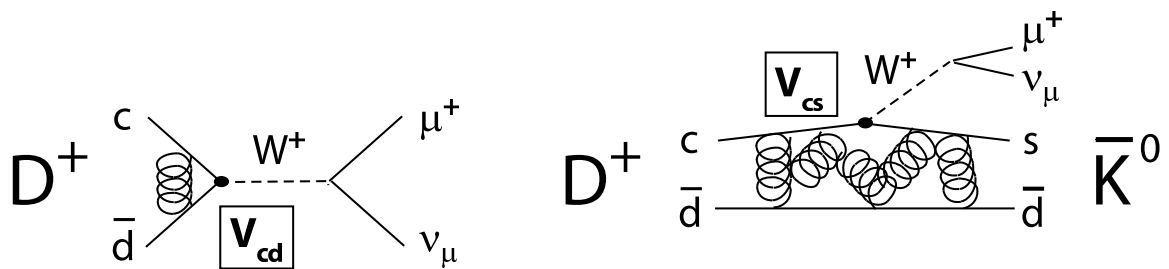


Figure 1: Diagrams for the reactions $D^+ \rightarrow \mu^+ \nu_\mu$ and $D^+ \rightarrow \bar{K}^0 \mu^+ \nu_\mu$.

The strong interaction of the participating quarks introduces a complication because its effect is challenging to estimate accurately. Theory's difficulty in calculating phenomena rooted in strong physics seriously hamper some measurements related to weak physics in the B sector that need such input, for example extracting V_{ub} from semileptonic and leptonic B decays, or V_{td} from $B^0 - \bar{B}^0$ mixing. Theory tools have become available, but they require calibration or verification. The similarity of the charm and the bottom quark allow to test the same methods in D decay, where the quantities in question can be determined to excellent accuracy because the corresponding CKM matrix elements are well-constrained from other sources. In addition to being of interest in their own right, experimental charm results thus have a much larger impact on the field.

This presentation discusses leptonic and semileptonic D and D_s decays, where results from the BaBar, Belle, CLEO, and FOCUS collaborations are reported. The challenge in all these cases, aside from signal purity and background concerns in general, is to cleanly identify decays with neutrinos and to determine the kinematic properties of the undetected particle through external constraints.

The CLEO experiment benefits from the clean experimental environment that arises from running at or slightly above production threshold, $e^+e^- \rightarrow \psi(3770) \rightarrow D\bar{D}$ or $e^+e^- \rightarrow D_s^*\bar{D}_s \rightarrow \gamma D_s\bar{D}_s$. Identifying one of the $D_{[s]}$ by reconstructing its decay to a well-identified final state ("tagging") already guarantees a second $D_{[s]}$ in the event, which is then analyzed for a particular reaction. Because of the known final state in the first step, it is also possible to not require a tag, but to add all reconstructed tracks and showers to infer the neutrino momentum. Finally, and of particular importance, the experimental set-up also allows to count the number of produced decays accurately, thereby facilitating absolute normalization.

The B factories usually use the continuum process $e^+e^- \rightarrow c\bar{c}$ at center-of-mass energies near the $\Upsilon(4S)$. They obtain D mesons via the decay chain $D^* \rightarrow \pi_s D$, where π_s is a slow pion to mark the D flavor. It is possible to analyze both D^+ and D^0 in this way, but in practice, this method is mostly applied to $D^{*+} \rightarrow \pi_s^+ D^0$, which also has the most favorable branching fraction. Since determining the number of D decays produced in fragmentation is difficult, measurements are often performed relative to another $D_{[s]}$ decay mode. Tagging in this case means that the presence of one reconstructed D meson from $e^+e^- \rightarrow c\bar{c}$ does imply a second charm particle in the event (which then is the signal side). Even in the absence of a way to normalize the rate, it is still possible to compare the shape of kinematic distributions with theoretical predictions, for example form factor shapes (see below).

2 Leptonic Decays

Leptonic D decays proceed through annihilation of the constituent quarks into a W , followed by its decay into a lepton and the corresponding neutrino. The partial width for $\ell = e, \mu$, and τ is given by

$$\Gamma(D^+ \rightarrow \ell^+ \nu_\ell) = \frac{1}{8\pi} G_F^2 f_D^2 m_\ell^2 M_D \left(1 - \frac{m_\ell^2}{M_D^2}\right)^2 |V_{cd}|^2, \quad (1)$$

where f_D is the D meson decay constant and m_ℓ and M_D are the lepton and D meson masses. G_F is the Fermi coupling constant. For D_s decay, the mass of the D_s , the decay constant of f_{D_s} , and V_{cs} are used instead. A similar formula applies for $B_{[s]}$ decays. The quantities determined in leptonic $D_{[s]}$ decays are the charm decay constant, given that the masses and the CKM elements are well-measured. The decay constant describes the strong interaction surrounding the annihilation process.

Experimental accuracy in the few-percent range is crucial to validate calculations of the decay constant in both the charm and the bottom sector. Further goals are: comparing the lepton species to put limits on physics beyond the Standard Model, and determining f_{D_s}/f_D , where some technical uncertainties cancel. The Standard Model predicts the following ratios for the production rate of $\tau : \mu : e$:

$$D \rightarrow \ell \nu_\ell : \quad 9.72 : 1 : 0.00002, \quad D_s \rightarrow \ell \nu_\ell : \quad 2.65 : 1 : 0.00002. \quad (2)$$

In principle, it is possible to determine the decay constants from decays to all three lepton species. A few experimental considerations to take into account: $D_{[s]}^+ \rightarrow e^+ \nu_e$ is beyond current experimental reach (low branching fraction due to helicity suppression). $D_{[s]}^+ \rightarrow \tau^+ \nu_\tau$ is most copiously produced, but the observed rate is lowered, and the measurement complicated by, the subsequent decay of the τ , which involves at least one more neutrino. $D_{[s]}^+ \rightarrow \mu^+ \nu_\mu$ is therefore the experimentally accessible.

2.1 Leptonic D decays

CLEO studied the decay $D^+ \rightarrow \mu^+ \nu_\mu$ in 281 of $\psi(3770)$ data using the tagging technique [1]. The decay is identified with a single muon-like track on the signal side, and candidate events are required to have a missing mass squared near zero. The missing mass squared is calculated using the beam energy E_{beam} , the muon energy and momentum E_{μ^+} and p_{μ^+} , and the momentum p_D of the D : $MM^2 = (E_{\text{beam}} - E_{\mu^+})^2 - (-p_{D^-} - p_{\mu^+})^2$, which for signal events corresponds to the neutrino mass. The signal distribution is shown in Fig. 2. Fifty signal candidates are found, with 2.8 background events (mostly D^+ decay to $\pi^+ \pi^0$, $\tau^+ (\rightarrow \pi^+ \nu)$, and $K^0 \pi^+$ tails from the well-separated peak at higher MM^2) expected. This allows measurement of the branching fraction $\mathcal{B}(D^+ \rightarrow \mu^+ \nu_\mu) = (4.4 \pm 0.7 \pm 0.1) \times 10^{-4}$ and hence $f_D = (222.6 \pm 16.7_{-3.4}^{+2.8})$, with V_{cd} as an external input. With the SM ratios from Eqn. 2 applied to the measured branching fraction $\mathcal{B}(D^+ \rightarrow \mu^+ \nu_\mu)$, one expects $\mathcal{B}(D^+ \rightarrow e^+ \nu_e) \sim 1 \times 10^{-8}$ and $\mathcal{B}(D^+ \rightarrow \tau^+ \nu_\tau) \sim 2 \times 10^{-3}$. Slight modification of the signal side selection criteria gives access to $\ell = e, \tau$, by asking for either an electron-like track (no events seen, $\mathcal{B}(D^+ \rightarrow e^+ \nu_e) < 2.4 \times 10^{-5}$), or by asking for a pion track and a missing mass shifted away from zero, signalling the decay $\tau \rightarrow \pi \nu$ (no significant signal, $\mathcal{B}(D^+ \rightarrow \tau^+ \nu_\tau) < 3.1 \times 10^{-3}$).

2.2 Leptonic D_s decays

Both BaBar and CLEO have recently studied leptonic D_s decays. BaBar bases their study on 230 of data in the $\Upsilon(4S)$ region. They use kinematic constraints, require an identified D^0, D^+, D^{*+} , or D_s^+ , and use the signal side decay chain $D_s^{*+} \rightarrow \gamma D_s^+$, $D_s^+ \rightarrow \mu^+ \nu_\mu$ to provide a clean D_s sample [4] (extra particles may be present in

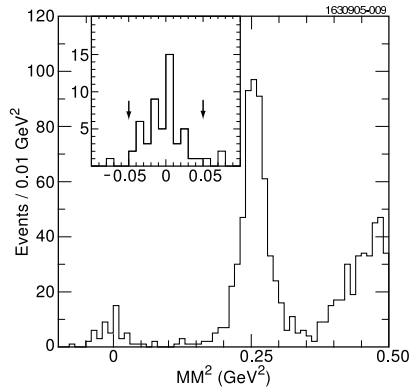


Figure 2: $D^+ \rightarrow \mu^+ \nu_\mu$: reconstructed neutrino mass for signal events [1].

the event). The neutrino momentum is inferred from all other measured reaction products. The signal distribution is the $D_s^* - D_s$ mass difference $m(\gamma\mu^+\nu_\mu) - m(\mu^+\nu_\mu)$, shown in Fig. 3. Since the D_s^* production rate is not precisely known, BaBar determine the ratio relative to $D_s^+ \rightarrow (K^+K^-)\pi^+$ with $m(K^+K^-)$ in the ϕ mass region ($\pm 2\Gamma_\phi$), $\Gamma(D_s^+ \rightarrow \mu^+\nu_\mu)/\Gamma(D_s^+ \rightarrow \phi\pi^+)$. With $\mathcal{B}(D_s^+ \rightarrow \phi\pi^+) = (4.71 \pm 0.46)\%$ [5] they arrive at $\mathcal{B}(D_s^+ \rightarrow \mu^+\nu_\mu) = (6.74 \pm 0.83 \pm 0.26 \pm 0.66) \times 10^{-3}$, where the third error is due to the normalization uncertainty. This leads to $f_{D_s} = (283 \pm 17 \pm 7 \pm 14)$.

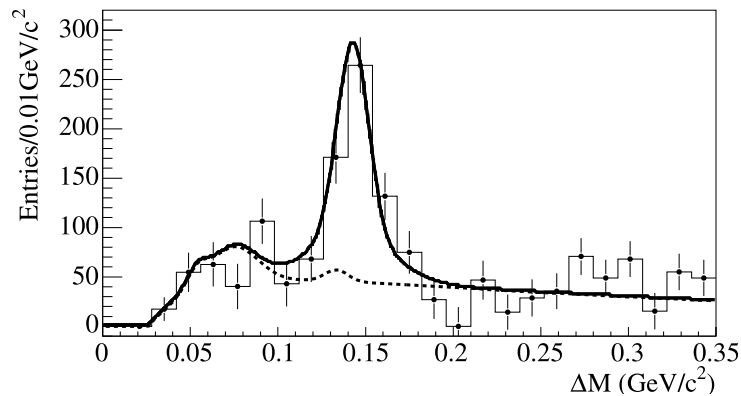


Figure 3: BaBar's signal distribution $\Delta M = m(\gamma\mu^+\nu_\mu) - m(\mu^+\nu_\mu)$ for the decay $D_s^+ \rightarrow \mu^+\nu_\mu$ detected in $D_s^* \rightarrow \gamma D_s$ [4]. The structure at $\Delta M \sim 0.07/c^2$ is due to the decay $D_s^* \rightarrow \pi^0 D_s$; the peak underneath the signal in the background shape is due to $D_s^+ \rightarrow \tau\nu_\tau$.

CLEO's analysis relies on ~ 200 of data taken at a center-of-mass energy of 4170. The decay chain is $e^+e^- \rightarrow D_s^* \bar{D}_s \rightarrow (\gamma D_s) \bar{D}_s$. One D_s is tagged, the other is

analyzed for the signal decay. Two strategies are used.

A. As above, the missing mass squared is examined to identify the signal. The lone signal side track is required to not be an electron but instead to be muonic or pionic. An energy requirement of 300 accepts 99% of all muon tracks and 60% of all pion tracks. We distinguish cases with an energy deposition below 300 in the calorimeter (typical for $D_s^+ \rightarrow \mu^+\nu_\mu$, but possible for $\tau \rightarrow \pi\nu_\tau$) from those that have above 300 (in which case the track is likely to be a pion from $\tau \rightarrow \pi\nu_\tau$). The data show a clear enhancement in the expected $D_s^+ \rightarrow \mu^+\nu_\mu$ signal region. The $D_s^+ \rightarrow \tau\nu_\tau$ events are more spread out due to the presence of the additional, unreconstructed, neutrino, but signal events are seen as well. The signatures for $\ell = \mu$ and τ overlap, hence the summed distribution is fit for the two branching fractions, where the SM ratio for the two is assumed. CLEO's preliminary result, combining the two, is $\mathcal{B}(D_s^+ \rightarrow \mu^+\nu_\mu) = (0.664 \pm 0.076 \pm 0.028)$, or $f_{D_s} = (282 \pm 16 \pm 7)$. If the track is required to be consistent with an electron, no candidates are found, resulting in an upper limit of $\mathcal{B}(D_s^+ \rightarrow e^+\nu_e) < 3.1 \times 10^{-4}$.

B. The second approach, based on the same data, uses the decay chain $\tau \rightarrow e\bar{\nu}_e\nu_\tau$. Its product with the $D_s^+ \rightarrow \tau^+\nu_\tau$ branching fraction ($\sim 6 - 7\%$) is about 1.3%, to be compared with the inclusive semileptonic branching ratio $D_s^+ \rightarrow Xe^+\nu_e \sim 8\%$. The analysis procedure demands a sole electron-like track on the signal side, and limits the energy not associated with the other identified decay products in the calorimeter to be less than 400. No additional energy deposition is expected for signal events other than the transition photon from $D_s^*\bar{D}_s \rightarrow (\gamma D_s)\bar{D}_s$, upon which no selection requirements are placed, and showers resulting from interactions of the decay products of the tag side with the detector material. The signal distribution, together with background estimates from Monte Carlo simulations, is presented in Fig. 4. This analysis leads to $\mathcal{B}(D_s^+ \rightarrow \tau^+\nu_\tau) = (6.3 \pm 0.8 \pm 0.5)\%$ and $f_{D_s} = (278 \pm 17 \pm 12)$ (both preliminary). Since the two measurements are complementary, one can form the average $f_{D_s} = (280 \pm 12 \pm 6)$ and also use them to measure the ratio $\mathcal{B}(D_s^+ \rightarrow \tau^+\nu_\tau) : \mathcal{B}(D_s^+ \rightarrow \mu^+\nu_\mu) = (9.9 \pm 1.9)$, consistent with the SM expectation of 9.72.

2.3 Leptonic Decays: Summary

A visual comparison of current experimental and theoretical progress on the decay constants is given in Fig. 5. In summary: f_D from $D^+ \rightarrow \mu^+\nu_\mu$ is measured to a total relative error of 8%; the decays to e and τ are presently not experimentally accessible, although the current upper limit gives rise to the hope that a signal will soon be within reach for τ . The decay constant f_{D_s} has been measured in $D_s^+ \rightarrow \mu^+\nu_\mu$ (BaBar, CLEO) and $D_s^+ \rightarrow \tau^+\nu_\tau$ (CLEO) to an accuracy of 5-8%. The precision of theoretical calculations are in this region as well. However, the dominant experimental uncertainty is still statistical, which is – in principle – much easier to improve upon than systematic errors such as those theory is in the process of overcoming.

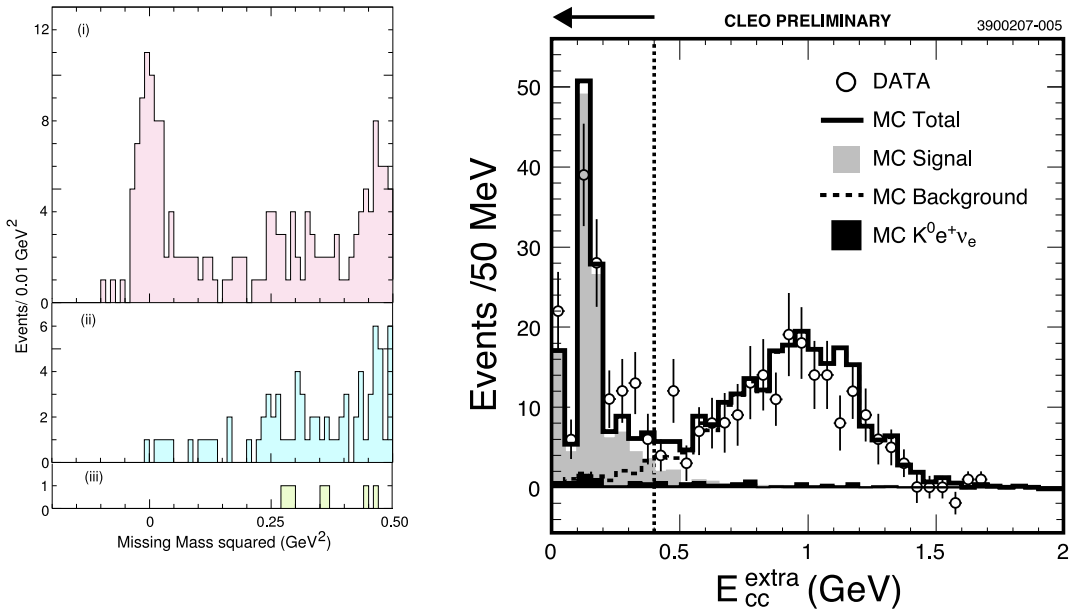


Figure 4: CLEO data on leptonic D_s decays (preliminary). Left: Missing-mass-squared distributions from data corresponding to (i) $D_s^+ \rightarrow \mu^+ \nu_\mu + \tau^+ \nu_\tau$, (ii) $D_s^+ \rightarrow \tau^+ \nu_\tau$, (iii) $D_s^+ \rightarrow e \nu_e$. Right: $D_s^+ \rightarrow \tau^+ \nu_\tau$: Energy deposited in the calorimeter for tagged D_s events and a single electron-like track on the signal side *not* accounted for by the tag or the electron candidate. The circles are data; the curves are MC predictions for signal as well as several semileptonic background sources.

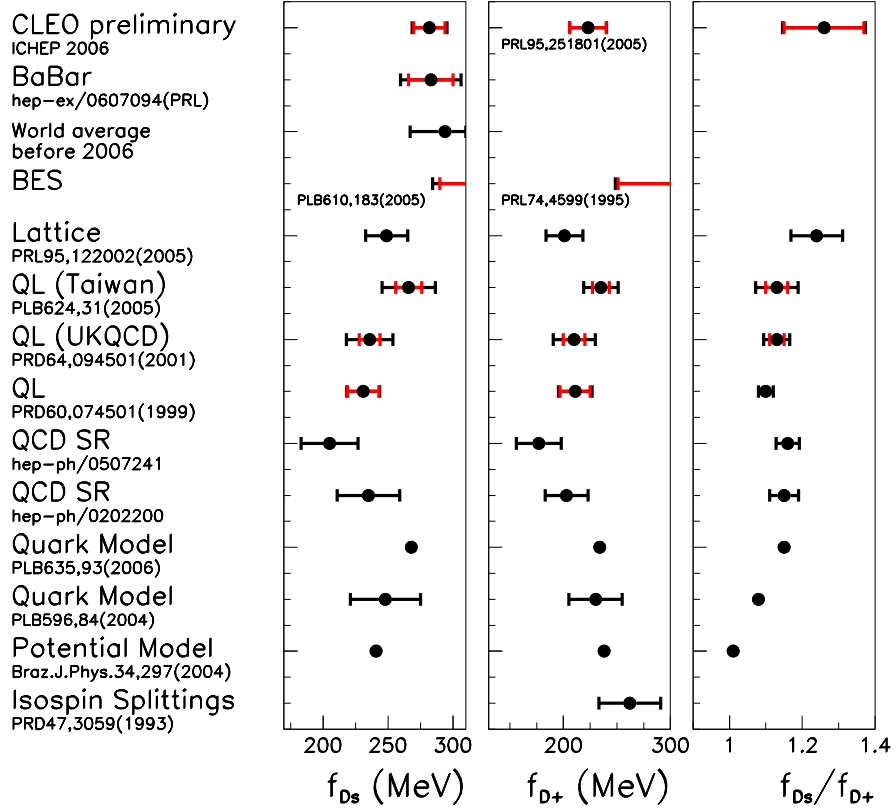
3 Semileptonic Decays

Semileptonic decays $D \rightarrow h \ell \nu_\ell$ provide yet another scenario within which to study the impact of strong force. The underlying weak process at the quark level, for instance $c \rightarrow W^* q$ with $W^* \rightarrow e \nu$, can be calculated, but the observed rate is modified by the QCD interaction between the participant as well as the spectator quarks, which clouds the simple picture.

3.1 Branching fractions

The current experimental uncertainty on the $D \rightarrow K, \pi e \nu$ branching fractions is in the percent regime, thereby posing a challenge to the precision of the LQCD predictions [12].

The search is on for rarer modes, and CLEO have improved considerably upon previously achieved accuracy in many modes (Table 1). $D^+ \rightarrow \eta e^+ \nu$ has been observed for the first time ($> 5\sigma$), as has the first multi-body semileptonic decay: $D^0 \rightarrow$

Figure 5: Recent experimental and theoretical results on f_D and f_{D_s} .

$K^-\pi^+\pi^-e^+\nu_e$ ($> 4\sigma$), which is found to mostly proceed via $K_1(1270)^- \rightarrow K^-\pi^+\pi^-$. The uncertainties on $D^+ \rightarrow \omega e^+\nu$ branching fraction have been halved, and the upper limits on the branching fractions $D^+ \rightarrow \eta', \phi e^+\nu$ have been tightened by two orders of magnitude. Once an $\eta' e \nu_e$ signal is observed this will allow a comparison with predictions for the ratio $D \rightarrow \eta : D \rightarrow \eta'$.

3.2 Form factors

Decay to a pseudoscalar

The dynamics of semileptonic $D \rightarrow h \ell \nu_\ell$ decays can for the case of a pseudoscalar hadron in the final state in the limit of small lepton masses be described as follows:

$$\frac{d\Gamma}{dq^2} \propto |f_+^h(q^2)|^2 \times p_h^3 \times |V_{cq}|^2, \quad (3)$$

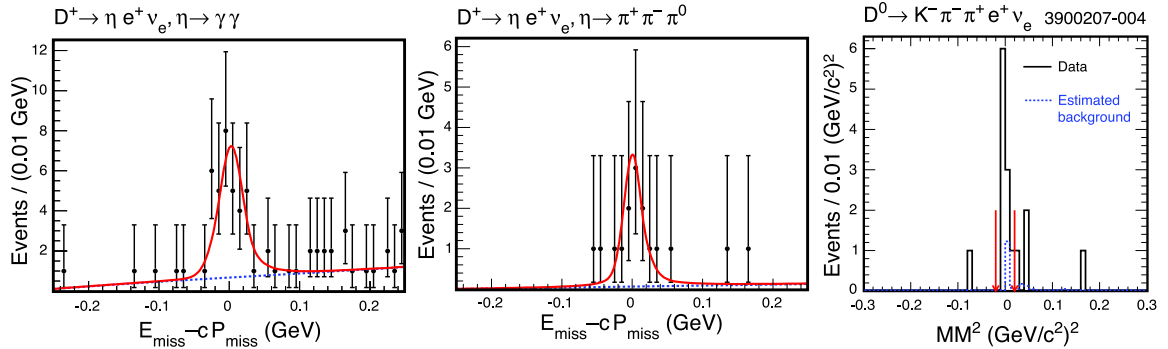


Figure 6: Preliminary CLEO results: Signal distributions for $D^+ \rightarrow \eta e^+ \nu$ for $\eta \rightarrow \gamma\gamma$ (left) and $\eta \rightarrow \pi^+ \pi^- \pi^0$ (middle); $D^0 \rightarrow K^- \pi^+ \pi^- e^+ \nu$.

where q^2 is the momentum transfer to the W^* , $f_+^h(q^2)$ is the form factor function describing the probability to end up with a hadron of type h in the final state for a given q^2 , p_h is the momentum of the outgoing hadron, and V_{cq} is the appropriate CKM matrix element.

Theoretical predictions for the form factor shape can be tested against the q^2 distribution in data, corrected for the q^2 -dependent detection efficiency. This is detailed further below. The normalization is determined by the product $|V_{cq}| \times f_+(0)$. Due to the precision with which V_{cs} and V_{cd} are determined in other experiments (2 – 4%), a measurement of $|V_{cq}| \times f_+(0)$ determines $f_+(0)$.

Examples of form factor determinations are displayed in Fig. 7. The simplest reasonable parametrization of the pseudoscalar form factor is the single pole shape, $\sim 1/(1 - q^2/M_{\text{pole}}^2)$ [10], where the nominal setting of the parameter is $M_{\text{pole}} = M(D_s^*)[M(D^*)]$ for $h = K[\pi]$. More sophisticated models are the modified pole model,

$$f_+^h(q^2) = \frac{f_+^h(0)}{(1 - \alpha q^2/M_{\text{pole}}^2) \times (1 - q^2/M_{\text{pole}}^2)}, \quad (4)$$

or, recently, the Hill series parametrization [11]. BaBar [13], Belle [15], CLEO [6], and FOCUS [14] compare their various results for $D \rightarrow \pi, K l \nu$ data for $D = D^{+,0}$ with the models and find reasonable agreement with all of them. In particular the Belle and CLEO measurements boast superb statistics and an excellent q^2 resolution. In general it is found that unquenched LQCD predicts the form factor shape a little too high especially for $D \rightarrow \pi$ [6, 15], but has achieved useful uncertainty, as visually evident from the agreement between the data points and the curve obtained from an interpolation between LQCD predictions at several q^2 points, Fig. 7. Fitting the predicted LQCD data points to the modified pole model shape, thereby extracting $f_+(0)$ and α , allows a comparison within this model between theory and the experiments.

This is presented for $f_+(0)$ in Fig. 8.

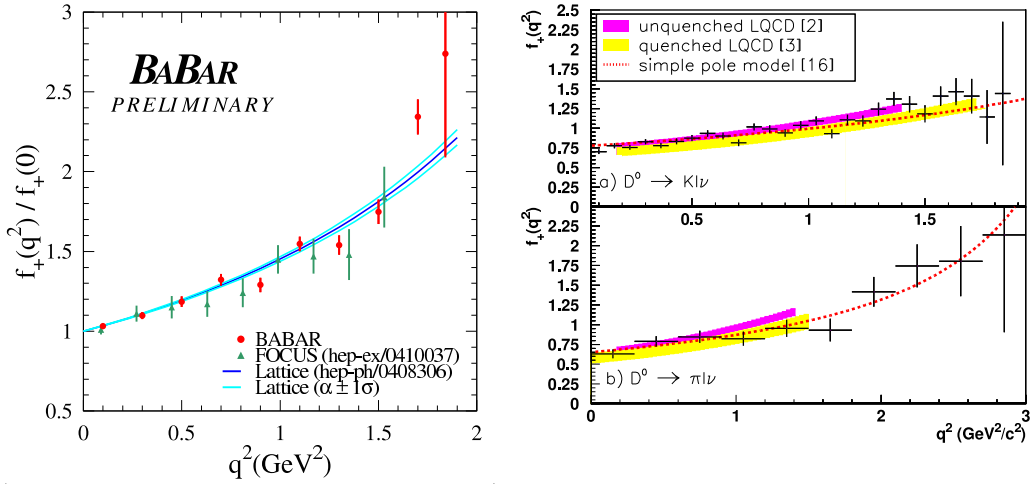


Figure 7: Form factor shapes. Left (from Ref. [13]): BaBar ($D \rightarrow K e \nu_e$, points) and FOCUS [14] (triangles, $D \rightarrow K \mu \nu_\mu$) data and an unquenched LQCD calculation [12] (band). Right (from Ref. [15]): Belle results on $D \rightarrow K$ (top) and $D \rightarrow \pi$ (bottom), with unquenched [12] and quenched [16] LQCD predictions overlaid.

Alternatively, using $f_+^{D \rightarrow \pi} = 0.64 \pm 0.03 \pm 0.06$ and $f_+^{D \rightarrow K} = 0.73 \pm 0.03 \pm 0.07$ from LQCD [12], the CKM matrix elements are found to be in good agreement with current world averages. However, the uncertainties ($\sim 10\%$ relative) on the form factor magnitudes dominate. This constitutes a check of the LQCD calculation.

Decay to a vector

For a vector hadron in the final state, such as $D \rightarrow K^* e \nu$ (Cabibbo-favored) or $D \rightarrow \rho e \nu$ (Cabibbo-suppressed), more form factor functions enter the stage. The decay amplitude can be described in a parameter-free way using helicity basis form factors as specified in Ref. [17]. However, the helicity form factors are hard to calculate; a more traditional approach is to just assume spectroscopic pole dominance and cast the expression for the amplitude into linear combinations of the following functions:

$$A_i(q^2) = \frac{A_i(0)}{1 - q^2/M_{A_i}^2} \quad (i = 1, 2), \quad V(q^2) = \frac{V(0)}{1 - q^2/M_V^2}. \quad (5)$$

The pole masses are often fixed to be $M_V = 2.1$, $M_{A_{1,2}} = 2.5$. If one then defines $R_V = V(0)/A_1(0)$ and $R_2 = A_2(0)/A_1(0)$, one ends up with only two free parameters, albeit at the expense of an assumed shape. The parameter-free approach in Ref. [17] circumvents this.

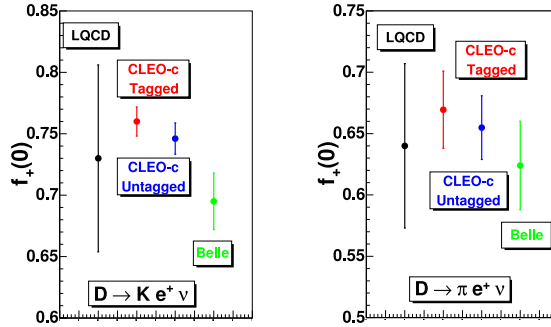


Figure 8: Comparison of form factor normalization for $D \rightarrow K$ and $D \rightarrow \pi$ obtained by unquenched LQCD [12], two CLEO [6] analyses, and Belle [15].

An analysis of $D^+ \rightarrow K^- \pi^+ e^+ \nu$ CLEO data uses a projective weighting technique, by which the expected shapes from helicity form factor contributions are fit to the data, thereby extracting the (bin-wise) amplitude for each of the form factors [18]. When the spectroscopic form factors as given in Eqn. 5, translated into helicity form factors, are overlaid, good agreement is found (Fig. 9). Additional conclusions are that a term describing interference with a non-resonant s -wave $K\pi$ component is necessary, and that no evidence is found for d - or f -wave contributions.

A recent preliminary study by BaBar [19] of $D_s^+ \rightarrow \phi e^+ \nu$, using about 13×10^3 signal events in 78.5, not only exhibits a beautifully precise measurement but also confirms an earlier FOCUS result. This actually resolves a controversy: The ratios R_V and R_2 for $D^+ \rightarrow K^* e^+ \nu$ and $D_s^+ \rightarrow \phi e^+ \nu$ are expected to be similar because the CKM matrix element involved is V_{cs} in both cases, and the only remaining difference is then the spectator quark flavor (\bar{d} vs. \bar{s}). Agreement within 10% is expected. This was not borne out by earlier data, which was not inconsistent for R_V but disagreed for R_2 , except for a FOCUS measurement [20] that had R_2^ϕ in agreement with the world average of $R_2^{K^*}$.

CLEO has presented preliminary results for the first Cabibbo-suppressed pseudoscalar \rightarrow vector form factor measurement, $D \rightarrow \rho e \nu$. A clear signal for both isospin states is observed, making it possible to bin in kinematic distributions. The branching fractions from the 281 data sample are found to be in good agreement with previous results (which are dominated by the CLEO-c results from the 56 sample, see Table 1), as is the partial width $D^0 \rightarrow \rho^- e^+ \nu = (0.41 \pm 0.03 \pm 0.02) \times 10^{-2}$. A simultaneous fit to $D^+ \rightarrow \rho^0 e^+ \nu_e$ and $D^0 \rightarrow \rho^- e^+ \nu_e$ (linked through isospin) results in the following determinations: $R_V^\rho = 1.40 \pm 0.25 \pm 0.03$, $R_2^\rho = 0.57 \pm 0.18 \pm 0.06$.

$D \rightarrow \rho e \nu$ and $D \rightarrow K^* e \nu$ studies are important to the B sector for example by aiding in the extraction of $|V_{ub}|^2/|V_{ts}|^2$ through $d\Gamma(B \rightarrow \rho e \nu) : d\Gamma(B \rightarrow K^* \ell \ell)$ [9],

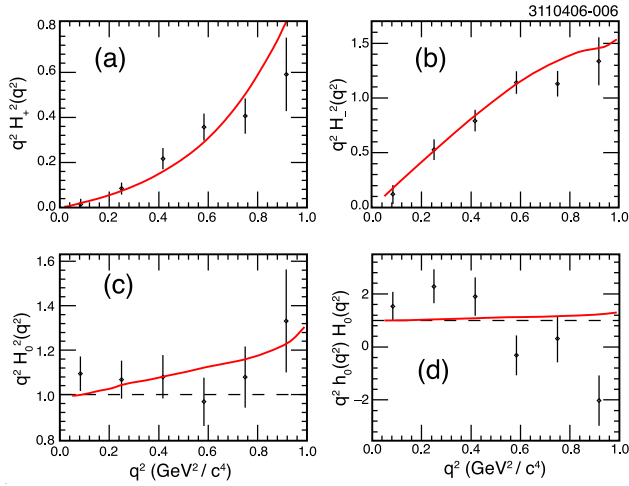


Figure 9: $D \rightarrow K\pi e\nu$ [18]: Four parameter-free helicity-basis form factor products as extracted in CLEO data, overlaid with form factors constructed from spectroscopic pole model shapes using $R_0 = 1.505$, $R_2 = 0.875$, and s -wave parameters $\mathcal{A} = 0.33$ and $\delta = 39^\circ$.

which requires either measurement of the $B \rightarrow \rho$ and $B \rightarrow K^*$ form factors or a calculation validated by the corresponding D decays.

3.3 Inclusive semileptonic decays

CLEO has determined the semileptonic inclusive branching fraction $D \rightarrow X e^+ \nu_e$ for both charged and neutral D mesons [21]. The measured branching fractions $\mathcal{B}(D^0 \rightarrow X e^+ \nu_e) = (6.46 \pm 0.17 \pm 0.13)\%$, $\mathcal{B}(D^+ \rightarrow X e^+ \nu_e) = (16.13 \pm 0.20 \pm 0.33)\%$ agree well with the sum of all exclusive modes, although there is room for as-yet-unobserved exclusive decays at the level of $\mathcal{B} \sim 10^{-3}$. Isospin symmetry is observed within errors for the inclusive semileptonic partial widths, $\Gamma_{D^+}/\Gamma_{D^0} = 0.985 \pm 0.028 \pm 0.015$.

Aside from the branching fraction, a quantity of interest is the electron momentum spectrum. Without weak annihilation contributions ($D^+ \rightarrow gW^+ \rightarrow X e^+ \nu$) agreement between the spectra from D^+ and D^0 is expected. Weak annihilation would modify the upper end of the electron spectrum. Within uncertainties, the D^0 and D^+ distributions agree (Fig. 11).

3.4 Semileptonic decays: Summary

Many new results on D branching fractions and $D \rightarrow P, V$ and $D_s \rightarrow V$ form factors have become available. Of particular interest are the shape and the normalization of the form factor functions. Experimental accuracy is at present still consistent with

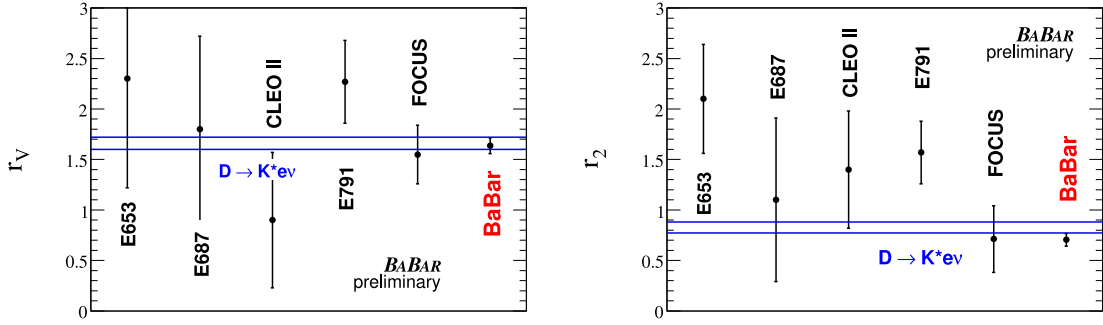


Figure 10: Comparison of form factor parameters R_2 (left) and R_V (right) for $D \rightarrow K^*$ and $D_s \rightarrow \phi$ semileptonic decays, from Ref. [19]. The data points all represent $D_s \rightarrow \phi$ analyses. The lines give the $\pm 1\sigma$ band for an average of experimental $D \rightarrow K^*$ results.

most calculations on the market; this may change as the experimental and theoretical uncertainties decrease.

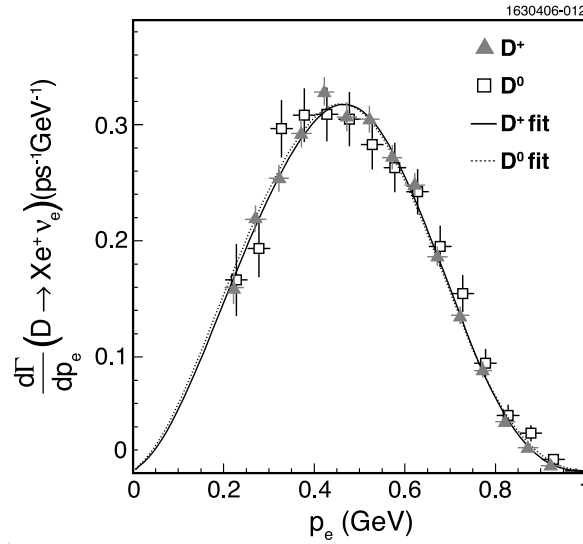


Figure 11: Electron momentum spectrum in $D \rightarrow X e^+ \nu_e$ for charged and neutral D mesons [21].

4 Conclusions

Precise results in the D sector have improved our comprehension of the QCD effects accompanying weak interactions and allowed to sharpen theoretical tools. Thanks to the similarity of the heavy quarks c and b , common calculation techniques can be applied to the estimation of D and B decay properties. Further progress in the D sector and consequently the B sector is in sight as data samples with modern detectors are being enlarged.

5 Acknowledgements

I would like to thank the conference organizers for an enjoyable conference at a exceptionally interesting venue. I am further indebted to many of my colleagues on CLEO, BaBar, Belle and FOCUS for helpful discussions. This work was supported by the US National Science Foundation under cooperative agreement PHY-0202078.

Decay	result (10^{-2})	PDG06 (10^{-2})	PDG04 (10^{-2})
$D^+ \rightarrow \bar{K}^0 \ell^+ \nu$	T: $8.86 \pm 0.17 \pm 0.20$ U: $8.75 \pm 0.13 \pm 0.30$	8.9 ± 0.4	6.8 ± 0.8
$D^0 \rightarrow K^- \ell^+ \nu$	T: $3.58 \pm 0.05 \pm 0.05$ U: $3.56 \pm 0.03 \pm 0.11$ Belle: $3.45 \pm 0.07 \pm 0.20$	3.41 ± 0.09	3.43 ± 0.14
$D^+ \rightarrow \pi^0 \ell^+ \nu$	T: $0.397 \pm 0.027 \pm 0.028$ U: $0.383 \pm 0.025 \pm 0.016$	0.44 ± 0.07	0.31 ± 0.15
$D^0 \rightarrow \pi^+ \ell^+ \nu$	T: $0.309 \pm 0.012 \pm 0.006$ U: $0.301 \pm 0.011 \pm 0.010$ Belle: $0.255 \pm 0.019 \pm 0.016$	0.27 ± 0.02	0.36 ± 0.06
$D^+ \rightarrow \rho^0 \ell \nu$	T: $0.232 \pm 0.020 \pm 0.012$	0.24 ± 0.04	0.31 ± 0.06
$D^0 \rightarrow \rho^+ \ell \nu$	T: $0.156 \pm 0.016 \pm 0.009$	0.19 ± 0.04	–
Decay	CLEO result (10^{-4})	PDG06 (10^{-4})	PDG04 (10^{-4})
$D^+ \rightarrow \omega \ell^+ \nu$	$14.9 \pm 2.7 \pm 0.5$	16_{-6}^{+7}	–
$D^+ \rightarrow \phi \ell^+ \nu$	< 2 (90% CL)	< 209	< 209
$D^+ \rightarrow \eta \ell^+ \nu$	$12.9 \pm 1.9 \pm 0.7$	< 70	< 50
$D^+ \rightarrow \eta' \ell^+ \nu$	< 3 (90% CL)	< 110	< 110
$D^0 \rightarrow K^- \pi^+ \pi^- \ell^+ \nu$	$2.9_{-1.0}^{+1.9} \pm 0.5$	< 12	< 12
$D^0 \rightarrow K_1(1270) \ell^+ \nu$	$2.2_{-1.0}^{+1.4} \pm 0.2$	–	–

Table 1: CLEO’s preliminary [6] and Belle’s published [15] measurements for D semileptonic branching fractions, and comparison with PDG06 [7] as well as PDG04 [8]. The PDG06 results include CLEO’s published numbers based on 56 of data taken at the $\psi(3770)$. “T” and “U” stand for CLEO’s “tagged” and “untagged” analyses, respectively, and the corresponding entries are not to be averaged because of sample overlap. CLEO’s results are all obtained with $\ell = e$, Belle’s with $\ell = e$ or μ , and the PDG numbers are averaged over e and μ , where available.

Bibliography

- [1] M. Artuso *et al.* [CLEO Collaboration], Phys. Rev. Lett. **95**, 251801 (2005) [arXiv:hep-ex/0508057].
- [2] P. Rubin *et al.* [CLEO Collaboration], Phys. Rev. D **73**, 112005 (2006) [arXiv:hep-ex/0604043].
- [3] S. Stone (CLEO Collaboration), contributed to the *33rd International Conference on High-Energy Physics (ICHEP06)*, Moscow, Russia, July 28 - August 2, 2006, arXiv:hep-ex/0610026.
- [4] B. Aubert *et al.* [BABAR Collaboration], arXiv:hep-ex/0607094 (submitted to Phys. Rev. Lett.).
- [5] B. Aubert *et al.* [BaBar Collaboration], Phys. Rev. D **71**, 091104 (2005) [arXiv:hep-ex/0502041]; B. Aubert *et al.* [BABAR Collaboration], Phys. Rev. D **74**, 031103 (2006) [arXiv:hep-ex/0605036].
- [6] Y. Gao [CLEO Collaboration], contributed to the *33rd International Conference on High-Energy Physics (ICHEP06)*, Moscow, Russia, July 28 - August 2, 2006.
- [7] W. M. Yao *et al.* [Particle Data Group], J. Phys. G **33**, 1 (2006).
- [8] S. Eidelman *et al.* [Particle Data Group], Phys. Lett. B **592**, 1 (2004).
- [9] B. Grinstein and D. Pirjol, Phys. Lett. B **549**, 314 (2002) [arXiv:hep-ph/0209211].
- [10] See e.g. P. L. Frabetti *et al.* [E687 Collaboration], Phys. Lett. B **364**, 127 (1995).
- [11] T. Becher and R. J. Hill, Phys. Lett. B **633**, 61 (2006) [arXiv:hep-ph/0509090].
- [12] C. Aubin *et al.*, Phys. Rev. Lett. **95**, 122002 (2005) [arXiv:hep-lat/0506030].
- [13] B. Aubert *et al.* [BABAR Collaboration], contributed to the *33rd International Conference on High-Energy Physics (ICHEP06)*, Moscow, Russia, July 28 - August 2, 2006, arXiv:hep-ex/0607077.
- [14] J. M. Link *et al.* [FOCUS Collaboration], Phys. Lett. B **607**, 233 (2005) [arXiv:hep-ex/0410037].
- [15] L. Widhalm *et al.*, Phys. Rev. Lett. **97**, 061804 (2006) [arXiv:hep-ex/0604049].
- [16] A. Abada, D. Becirevic, P. Boucaud, J. P. Leroy, V. Lubicz and F. Mescia, Nucl. Phys. B **619**, 565 (2001) [arXiv:hep-lat/0011065].

- [17] J. M. Link *et al.* [FOCUS Collaboration], Phys. Lett. B **633**, 183 (2006) [arXiv:hep-ex/0509027].
- [18] M. R. Shepherd *et al.* [CLEO Collaboration], Phys. Rev. D **74**, 052001 (2006) [arXiv:hep-ex/0606010].
- [19] B. Aubert *et al.* [BABAR Collaboration], contributed to the *33rd International Conference on High-Energy Physics (ICHEP06)*, Moscow, Russia, July 28 - August 2, 2006, arXiv:hep-ex/0607085.
- [20] J. M. Link *et al.* [FOCUS Collaboration], Phys. Lett. B **586**, 183 (2004) [arXiv:hep-ex/0401001].
- [21] N.E. Adam *et al.* [CLEO Collaboration], Phys. Rev. Lett. **97**, 251801 (2006) [arXiv:hep-ex/0604044].